Continental Shelf Research 165 (2018) 37–50

Contents lists available at ScienceDirect

Continental Shelf Research

journal homepage: www.elsevier.com/locate/csr

Hydro- and sediment dynamics in the Gironde estuary (France): Sensitivity to seasonal variations in river inflow and sea level rise

Barend van Maanen[a,b,*], Aldo Sottolichio[b]

[a] Faculty of Geosciences, Utrecht University, Princetonlaan 8A, 3584 CB Utrecht, The Netherlands
[b] University of Bordeaux, EPOC, UMR 5805, F33600 Pessac, France

ARTICLE INFO

Keywords:
Estuarine dynamics
Turbidity maximum
Sea level rise
Numerical modelling
Gironde estuary

ABSTRACT

Understanding estuarine hydrodynamics and sediment dynamics is of key importance to provide the foundation for sound management of these coastal systems. Turbidity maxima, which are zones of elevated suspended sediment concentration (SSC), are of particular interest as they control biogeochemical cycling and affect the overall environmental quality of the estuary. These turbidity maxima, however, are complex dynamic features that respond to changes in forcing conditions. In this study we use a 3D numerical model to investigate the response of hydrosedimentary dynamics to variations in river inflow and sea level rise in the Gironde estuary, which is one of the largest estuarine systems in Europe. Yearly simulations and comparisons with satellite data and measurements of salinity and SSC show that the model reproduces variations in salinity intrusion and the migration of the turbidity maximum driven by seasonal fluctuations in river inflow. Numerical experiments indicate that the formation of this dynamic turbidity maximum is mainly driven by tidal asymmetry. Density gradients play a secondary role by maintaining the stability of the suspended sediment mass. The model also simulates the presence of a secondary turbidity maximum which is more stable, consistent with observations. Evaluation of the sediment budget shows that sediment export mainly occurs during spring tides and when river discharge is high. Simulations including sea level rise suggest that salinity levels in the middle estuary will increase and rising water levels cause tidal amplification, strengthening of tidal currents and enhanced SSC levels in the upper estuary. On the other hand, the locations of the salinity front and the turbidity maximum remain relatively stable under rising water levels. Overall, our simulations suggest that decadal changes in river inflow can potentially have a larger effect on turbidity maximum dynamics than sea level rise.

1. Introduction

Estuaries are found along many parts of the world's coastline. These environments form the transition between riverine systems and the sea, creating highly energetic and dynamic sedimentary environments with large spatial and temporal gradients in physical properties, such as salinity and suspended sediment concentration (SSC) (Dyer, 1997). A characteristic feature in estuarine systems is the formation of a turbidity maximum. These turbidity maxima are zones of locally-elevated suspended matter concentration and understanding their dynamics and behaviour is of key importance for estuarine and coastal environmental issues. Indeed, the estuarine turbidity maximum plays a role in the long-term infilling of an estuary as well as it plays a notable role in biogeochemical cycles. Moreover, seaward fluxes are directly conditioned by residence times of suspended matter within the estuarine zone (Dyer, 1986).

Following the paradigm proposed by Dyer (1988), two main mechanisms can induce a turbidity maximum in tidal estuaries. Firstly, the transition between fresh and saline water leads to a density-driven residual circulation, with a seaward flow at the surface and a landward flow near the bottom that traps suspended material at the landward limit of the salinity intrusion (Postma, 1967). Secondly, the asymmetry of the tidal wave, in which the flood phase is shorter than the ebb phase, causes upstream tidal pumping (Uncles et al., 1984). The inequality between flood and ebb currents drives a net landward transport of suspended matter because of a more intense resuspension during the flood phase, and a more massive settling during high water slack, which is longer than low water slack (Allen et al., 1980). This tidal pumping of particles becomes ineffective once the river flow starts to dominate. Other processes that contribute to the formation of a turbidity maximum are suppression of turbulence by vertical density stratification (Simpson et al., 1990; Geyer, 1993) and tidal velocity asymmetry due to changes in vertical mixing during the tidal phase (Jay and Musiak, 1994). These mechanisms may apply to many

* Corresponding author at: Faculty of Geosciences, Utrecht University, Princetonlaan 8A, 3584 CB Utrecht, The Netherlands.
E-mail address: b.vanmaanen@uu.nl (B. van Maanen).

https://doi.org/10.1016/j.csr.2018.06.001
Received 5 May 2017; Received in revised form 29 May 2018; Accepted 2 June 2018
Available online 04 June 2018
0278-4343/

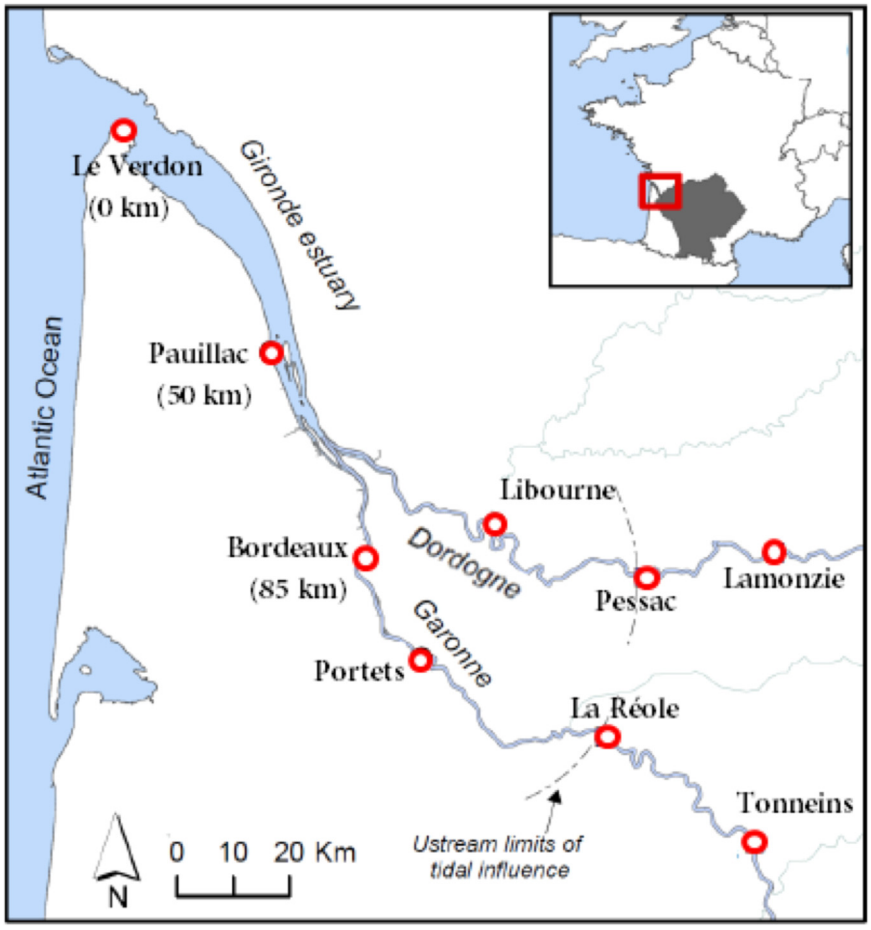

Fig. 1. Location map of the Gironde estuary. The grey area in the insert shows the watershed of Garonne and Dordogne rivers.

estuaries, and their relative importance is dependent on the characteristics of each environment, including shape and bathymetry, river flow, and particle behaviour. Even if many of these mechanisms can act together, we here focus on the two mechanisms of Dyer's paradigm, which is a first order approach on the identification of key factors (Brenon and Le Hir, 1999).

Here we study one of the largest estuaries in Europe, the Gironde located in southwest France (Fig. 1) where a well-developed turbidity maximum appears, and we take advantage of existing field data to compare to a numerical model. The Gironde estuary is a partially mixed to well-mixed macrotidal estuary with a relatively strong river discharge. Investigations into sediment dynamics in the Gironde estuary have highlighted the complexity of the formation of the turbidity maximum. Early observations pointed out that the high-concentration zone was always located close to the freshwater-saltwater interface (Allen, 1972), suggesting that density effects play a major role. However, Allen et al. (1980) later demonstrated that the origin of the turbidity maximum is tidally-induced. In addition to this tidally-induced turbidity maximum which shifts along the estuary depending on river flow, a secondary high turbidity zone in the Gironde exists which remains at a more steady location. Sottolichio and Castaing (1999) described both turbidity maxima based on suspended sediment distributions obtained from water sampling along transects. However, because of the large spatial scales involved these in-situ measurements can provide only limited quantitative information on the geometry and dynamics of these turbidity maxima. Satellite remote sensing can help to obtain a more complete picture of sediment dynamics in the whole estuary. Doxaran et al. (2009) used MODIS satellite data covering a 1-year period (Jan 2005 – December 2005) and they also detected the existence of two distinct turbidity maxima (Fig. 2). Although this type of satellite data improves our understanding of spatial distributions and movements, it remains difficult to use these images to elucidate underlying mechanisms and to make predictions on how sediment dynamics might change in the future under changing boundary conditions.

Both exploratory models (e.g. Huijts et al., 2006, 2009; Talke et al., 2009a; Chernetsky et al., 2010) and simulation models (e.g. Brenon and Le Hir, 1999; Cancino and Neves, 1999; Le Normant, 2000; Burchard et al., 2004; Park et al., 2008; Toublanc et al., 2016) (following the model classification by Murray, 2003) have been successfully applied to study hydrosedimentary processes in estuarine systems. For the Gironde, Sottolichio et al. (2001) conducted numerical modelling exercises to assess the mechanism responsible for the turbidity maximum formation. A 2DH model reproduced the right position of the turbidity maximum under tidal asymmetry effects only, confirming the main role of the tide. The use of a 3D model suggested that density stratifications cause a sharper seaward limit of the turbidity maximum. Sottolichio et al. (2001) pointed out that the conclusions presented in their paper were preliminary, as the parameterizations of particle behaviour and sediment processes were simplified and sedimentary patterns were only partly validated because of the lack of consistent data. Furthermore, they stressed the need to perform longer term simulations to evaluate trends in estuarine sediment budget.

Similar to Sottolichio et al. (2001), modelling efforts usually address estuarine dynamics over a relatively short time scale. Multiple simulations may then be carried out with different river flows to study the effect of freshwater discharge on the location of the salinity front and turbidity maximum (Brenon and Le Hir, 1999; Lin and Kuo, 2003). Simulations of salinity and turbidity over a complete year or longer, however, are still scarce, even though they allow for a more detailed

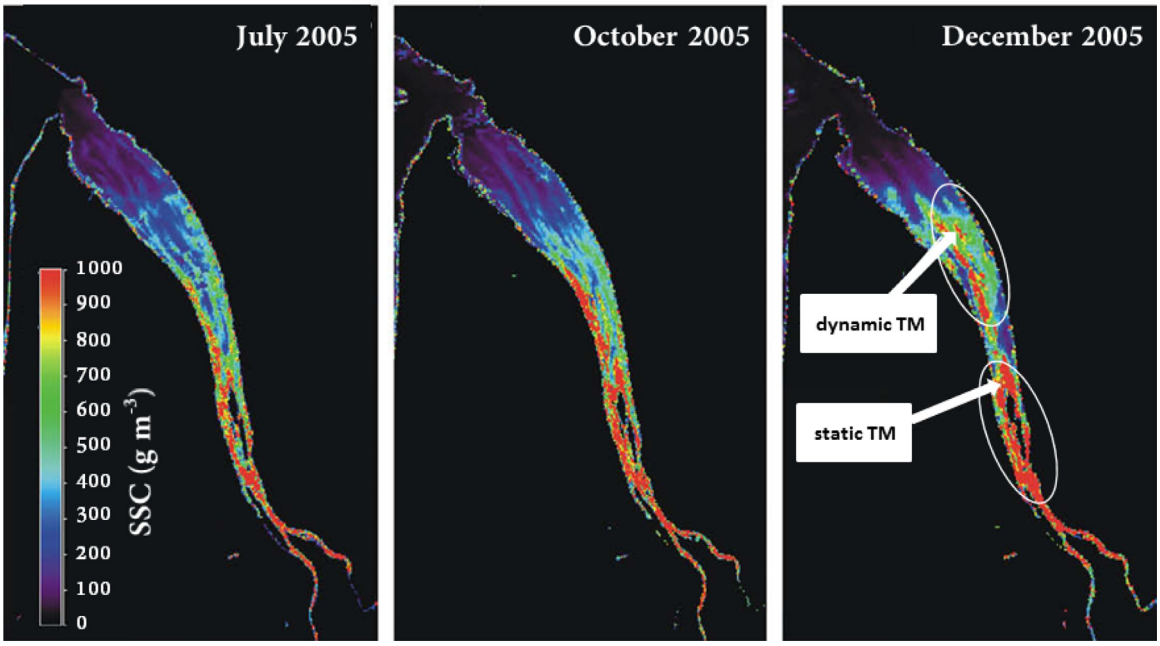

Fig. 2. Seasonal variations in turbidity derived from satellite imagery, showing a static turbidity maximum (TM) and a dynamic turbidity maximum which migrates in response to riverine input. Turbidity maps were produced from MODIS data recorded during spring conditions (adapted from Doxaran et al., 2009).

study of seasonal variations and can provide useful insight into large-scale sedimentary patterns and fluxes (Le Hir et al., 2001; Mitchell and Uncles, 2013). Apart from seasonal variations in river inflow, potential implications of changes in downstream boundary conditions linked to sea level rise require additional attention. Modelling studies have started to explore sea level rise effects and include an assessment of enhanced salt intrusion and modifications in the tidal propagation (Robins et al., 2016). So far, the main focus has been on these types of hydrodynamic implications (Rice et al., 2012; Chua and Xu, 2014). Sea level rise might also influence SSC patterns and turbidity maximum properties (Mitchell and Uncles, 2013) but these effects remain largely unexplored.

The first goal of our study is to investigate seasonal trends in salinity and SSC patterns in the Gironde estuary, including the movement of the salt front and turbidity maximum. We therefore conduct simulations with a period of 1–1.5 years so that large variations in river inflow are covered. At this temporal scale, sediment budgets, indicating seaward fluxes and the overall amount of sediment in suspension or deposited on the sea floor, become increasingly important. We compare model results with satellite data and a unique dataset comprising long-term time-series of measured salinity and turbidity at different locations in the estuary (Jalón-Rojas et al., 2015). The Gironde estuary is particularly interesting because of the presence of multiple turbidity maxima and the model is tested on its ability to reproduce these. Simulations are also used to provide a deeper understanding on the role of tidal asymmetry and estuarine circulation on turbidity maximum formation. Our second goal is to explore the effects of sea level rise on estuarine dynamics. We conduct a simulation with a 1.0 m sea level rise and study potential implications for salt intrusion, tidal propagation as well as SSC patterns and turbidity maximum location.

2. Study area

2.1. The Gironde estuary

The Gironde estuary is located in the Bay of Biscay on the southwest macrotidal coast of France. It forms a coastal plain estuary that originates at the Bec d'Ambès, at the confluence of the Garonne and Dordogne rivers (Fig. 1). It extends for 75 km up to the mouth, covering an area of 630 km^2. From the point of view of physical processes, it is more appropriate to consider the whole fluvio-estuarine system, as salt water penetrates into the tidal rivers and the tidal wave propagates about 170 km upstream, up to La Réole in the Garonne and up to Pessac in the Dordogne (Jouanneau and Latouche, 1981). The estuary shows a regular funnel shape, where width and cross sections increase exponentially in a seaward direction (Castaing and Allen, 1981). The maximum width, located near the mouth, is 12 km at high tide. The main navigation channel spreads along the left bank between Bordeaux and le Verdon, with a mean depth of 10 m and a mean width of 300 m. A secondary channel exists along the right bank, where depths are much smaller and which is separated from the navigation channel by a system of elongated bars and islands. The tidal range in the inlet varies from 1.5 m during neaps to 5.5 m during springs (Castaing and Allen, 1981). The mean combined river discharge of the Garonne and the Dordogne rivers (measured at La Réole and Pessac) is about 900 $m^3 s^{-1}$, with a well-defined flood season from November to May (maximum daily-averaged values exceeding 3000 $m^3 s^{-1}$) and a low flow period from June to October (daily-averaged values generally below 200 $m^3 s^{-1}$) (Coynel et al., 2004).

2.2. Sedimentary features

Abundant investigations were done on sedimentology and sedimentary processes in the Gironde estuary, where main features of the turbidity maximum have been described through in-situ measurements and anchor stations (Jouanneau and Latouche, 1981). The channel bed is dominated by mud and all the fine-grained sediment accumulating in the estuary is derived from fluvial sources (Castaing and Allen, 1981). The high turbidity zone is characterised by SSCs of about 1 $g l^{-1}$ and more (Allen et al., 1977). During slack water periods, and especially on neap tides, thick layers of fluid mud appear on the channel bottom, with concentrations up to 300 $g l^{-1}$ (Allen, 1972). Jouanneau and Latouche (1981) reported that 70% of the turbidity maximum particles can be trapped in the fluid mud during neap tide. Reported estimates of the total mobile fine sediment mass within the estuary vary between 4.4 ± 0.5 (Jouanneau, 1979) and 6 million tons (Allen et al., 1977). This amount includes both the turbidity maximum and fluid mud sediments. As the mean yearly input of suspended silt and clay is about

1–2.5 million tons (Schäfer et al., 2002), it is estimated that the estuarine water body contains the equivalent suspended mud mass of several years of fluvial sediment input.

3. Numerical modelling

3.1. Model description

In this study we apply the SiAM 3D hydrosedimentary model. SiAM 3D has been extensively applied to simulate the dynamics of the Seine estuary (Brenon and Le Hir, 1999; Cugier and Le Hir, 2002; Thouvenin et al., 2007; Waeles et al., 2007) and it was also used by Sottolichio et al. (2001) in their study of the Gironde. Detailed model descriptions, especially regarding hydrodynamics, can be found in Brenon and Le Hir (1999) and Cugier and Le Hir (2002). In this section we focus on providing an overview of how sediment dynamics are treated.

The SiAM 3D model solves the Navier Stokes equations with a free surface boundary condition, applying the hydrostatic assumption and using the Boussinesq approximation. Barotropic and baroclinic modes are separated in order to solve the momentum and the continuity equations (Brenon and Le Hir, 1999). This means that depth-averaged computations are performed to determine the water surface elevation and the vertically averaged velocities. The computed water level is introduced into the set of 3D equations, which are solved to obtain all the velocity components. In turn, the solution of the 3D equations provides the bottom friction and vertical dispersion terms as well as the density gradients to the depth-averaged part of the model. Density of water is deduced from salinity and suspended particle matter, neglecting the effect of temperature variations. To account for the effect of density stratification on turbulence damping, the turbulent viscosity and diffusivity are parameterized by using a local Richardson number (Cugier and Le Hir, 2002). The turbulence closure is based on the mixing length theory. SiAM 3D adopts a Cartesian irregular spacing in the horizontal direction and it uses real depth coordinates on the vertical axis.

The sediment transport model solves an advection-dispersion equation for the mass conservation of suspended sediment:

$$\frac{\partial C}{\partial t} + \frac{\partial uC}{\partial x} + \frac{\partial vC}{\partial y} + \frac{\partial (w + w_s)C}{\partial z} = \frac{\partial}{\partial x}\left(k_x \frac{\partial C}{\partial x}\right) + \frac{\partial}{\partial y}\left(k_y \frac{\partial C}{\partial y}\right) + \frac{\partial}{\partial z}\left(k_z \frac{\partial C}{\partial z}\right), \quad (1)$$

where C is the SSC, w_s is the settling velocity and k_x, k_y, and k_z are dispersion coefficients. When multiple sediment classes are used then Eq. (1) is computed for each class. Sediment exchanges with the bottom are accounted for through deposition (D) and erosion (E). The deposition term is calculated from the Krone (1962) formulation:

$$D = w_s C\left(1 - \frac{\tau}{\tau_{cd}}\right), \quad (2)$$

where τ is the bottom shear stress and τ_{cd} is the critical shear stress for deposition (no deposition when $\tau > \tau_{cd}$). In the initial study by Sottolichio et al. (2001) the settling velocity was kept constant. Here we determine settling velocity for each class as a function of the total SSC. We follow the formulation as proposed by Le Hir et al. (2001), which adopts a minimum $w_{s,min}$ and maximum settling velocity $w_{s,max}$ for each sediment class and accounts for both flocculation and hindered settling. The erosion term is given by the Partheniades (1965) formulation, which depends on the excess shear stress:

$$E = E_0\left(\frac{\tau}{\tau_{ce}} - 1\right), \quad (3)$$

where E_0 is the erosion constant and τ_{ce} is the critical shear stress for erosion (no erosion when $\tau < \tau_{ce}$). This critical shear stress depends on the surficial sediment dry density following a power law: $\tau_{ce} = a{\cdot}C_s^{\,b}$ where a and b are empirical constants with a value of 0.0015 and 1.0 respectively (Brenon and Le Hir, 1999). Sediment dry density is in turn influenced by consolidation processes. We here use a one-dimensional vertical multi-layer sedimentation model that is coupled to the sediment transport model. This consolidation model solves the sediment mass conservation equation (see also Le Hir and Karlikow, 1992):

$$\frac{\partial C_s}{\partial t} + \frac{\partial V_s C_s}{\partial z} = 0, \quad (4)$$

where C_s is thus the dry density and V_s is the sedimentation velocity which is calculated according to the soil porosity by using a power law: $V_s = k{\cdot}P_s^{\,m}$ where k and m are empirical constants with a value of 0.0001 and 50 respectively (Brenon and Le Hir, 1999). The consolidation model computes mud density profiles. The number of layers, the upper layer thickness and the total bed thickness vary according to deposition, erosion and consolidation (Brenon and Le Hir, 1999). Finally, it should be stressed that the bathymetry is assumed constant and bed level changes do not feed back into the characteristics of the tide. This is consistent with other hydrosedimentary modelling studies (e.g. Brenon and Le Hir, 1999; van Maren et al., 2015; Toublanc et al., 2016).

3.2. Model setup, initial conditions, boundary conditions and parameters

The computational grid covers an area of approximately 232 × 326 km and includes the Gironde estuary as well as a large part of the continental shelf of the Bay of Biscay. Fig. 3 shows a section of this computational grid, focusing on the estuarine area. An irregular rectilinear grid was adopted with mesh sizes varying from 300 × 200–18,500 × 20,000 m to obtain a fine resolution in the estuary (especially in regions where bathymetric gradients are important), while retaining a reasonable number of computational points.

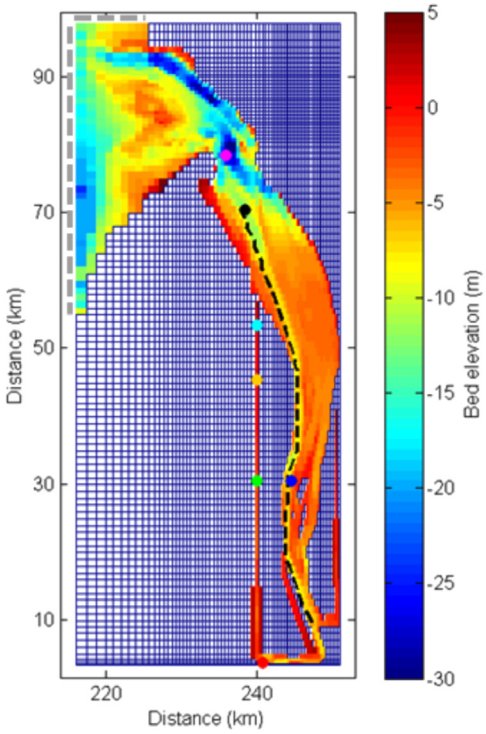

Fig. 3. Part of the computational grid, focusing on the estuarine area. The entire grid extends further offshore and includes a large part of the continental shelf of the Bay of Biscay. The paths of the Garonne and Dordogne rivers have been adapted to reduce the extent of the domain and limit computational cost without negative effects on model performance (similar to Brenon and Le Hir (1999) and Sottolichio et al. (2001)). The dashed black line indicates the location of the transect used for subsequent figures.

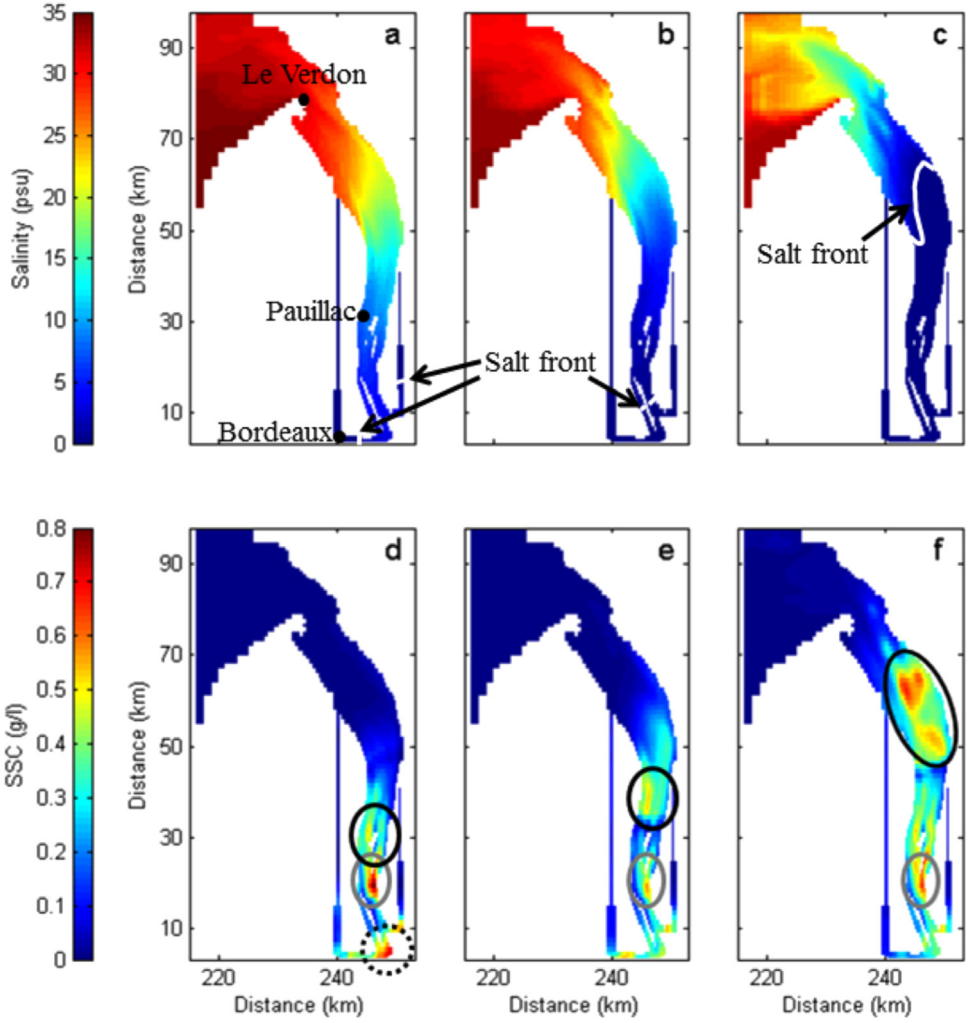

Fig. 4. Simulated salinity and turbidity fields during (a and d) low river discharge in July 2005, (b and e) intermediate river discharge in December 2005, and (c and f) high river discharge in March 2006. Salinity and turbidity fields are shown at low tide during spring conditions. Location of salt front is indicated. The black and grey ellipses indicate the dynamic and static turbidity maxima, respectively. The dotted ellipse indicates high turbidity levels in the Garonne river during low river flow conditions. Estuarine sediment mass predominantly consists of the coarser mud fraction.

Upstream of the confluence of the Garonne and Dordogne, grid cell width varies in order to respect the local mean width of the rivers. The water column was vertically split into horizontal layers that are 2 m thick in the estuary and thicker in the deeper zones. Along the seaward boundary, a real tide was imposed which was calculated as the sum of 21 harmonic components derived from long-term records at the shelf (Le Cann, 1990). The river inflows of the Garonne and Dordogne were introduced to the model every day at the upstream limits of the estuary.

Two classes of cohesive sediment are considered for the simulations presented here. For the reference simulation (as discussed in Section 4.1), $w_{s,min} = 1 \times 10^{-4}$ and $w_{s,max} = 1 \times 10^{-3}$ m/s for the finer mud fraction. For the coarser mud fraction, $w_{s,min} = 5 \times 10^{-4}$ and $w_{s,max} = 2 \times 10^{-3}$ m/s. Sensitivity of simulated sediment dynamics to the settling velocity will be discussed in Section 4.2.1. The erosion constant is set to 2×10^{-3} kg/m^2/s. The critical bottom stress for deposition is set to 10 N/m^2. Such a large value was also used by Brenon and Le Hir (1999) and Le Hir et al. (2001) and implies that deposition is always possible. This conceptualisation of deposition processes is in agreement with Winterwerp (2007) and is justified as consolidation is modelled and the erosion of unconsolidated deposits can instantaneously occur when turbulence is high enough (Le Hir et al., 2001). The simulations start with a total sediment budget of 3.84 million tons and this sediment is distributed over a number of grid cells in the navigation channel. This initial sediment mass fully consists of the coarser mud fraction. Input of sediment by the rivers is included by specifying a constant sediment concentration.

The model is calibrated to accurately reproduce the characteristics of tidal wave propagation by adjusting the roughness length distribution. Bottom friction is mainly varied in the longitudinal direction with z_0 values ranging between 10^{-4} and 10^{-2} m (lowest values are in the estuary itself and values progressively increase at the mouth and in the tidal rivers). The calibrated model is then applied to conduct long-term simulations of, as mentioned before, 1–1.5 years. The starting date of the simulations is set to 1 June 2005 given the availability of in-situ measurements for that period. An automatic continuous monitoring network (MAGEST) was implemented in the Gironde estuary in 2005 (Sottolichio et al., 2011). The network consists of four stations and each station continuously records salinity, temperature, dissolved oxygen, and SSC. Although some data is missing as a result of the network being out of service, this long-term dataset can be used for data-model comparisons and to further reveal variations in estuarine physical behaviour over seasonal cycling.

In the following section we will describe the results of model simulations. Model performance has been quantified by using the skill score introduced by Wilmott (1981) and commonly used in estuarine studies (e.g. Li et al., 2005; Warner et al., 2005; Hong and Shen, 2012; van Maren et al., 2015; Toublanc et al., 2016):

$$Skill = 1 - \frac{\sum |X_{\mathrm{mod}} - X_{obs}|^2}{\sum (|X_{\mathrm{mod}} - \overline{X_{obs}}| + |X_{obs} - \overline{X_{obs}}|)^2}, \quad (5)$$

where X_{mod} and X_{obs} are the modelled and observed variable and $\overline{X_{obs}}$ is the observed mean. Perfect agreement will yield a skill of 1 and complete disagreement will yield a skill of 0.

4. Modelling results

4.1. Salinity and SSC under seasonal variations in river inflow

4.1.1. Spatial distributions

The simulated period covers estuarine hydrosedimentary dynamics under both low and high flow conditions. That is, the daily averaged total river discharge ranges from about 160 to 5000 m^3/s so that the balance between riverine and tidal forcing varies considerably. It has been previously shown that the model accurately reproduces tidal forcing including characteristics such as tidal asymmetry and phase, and that it provides realistic flow fields (Sottolichio et al., 2001; Lajaunie-Salla et al., 2017). In this study, we focus on salinity and SSC patterns. To point out the importance of seasonal changes, we extracted the simulated salinity and SSC distributions at the water surface during different river flow conditions (Fig. 4). These simulated distributions are all shown at low tide and during spring conditions to allow for a fair comparison. With respect to salinity, seasonal variations can be clearly observed and the salt water intrusion is strongly dependent on river flow discharge. During low river flow (averaged monthly discharge: ~400 m^3/s), the salt front (defined here by the 0.5 psu isohaline) penetrates into the riverine systems of both the Garonne and Dordogne (Fig. 4a). On the other hand, the salt front is located in the lower part of the estuary in between Pauillac and le Verdon (Fig. 4c) during high river flow (averaged monthly discharge: ~1750 m^3/s). These seasonal fluctuations are also noticeable in the mouth of the estuary. Close to le Verdon, the salinity decreases from approximately 30 psu in July 2005 to less than 10 psu in March 2006, corresponding to the seaward transport of relatively low saline water by the increasing river discharge.

The simulated turbidity fields indicate that the model is capable of reproducing the formation of well-developed turbidity maxima (Fig. 4d, e, and f). The model reproduces the existence of a turbidity maximum which proves to be rather stable in position (indicated by the grey ellipses in Fig. 4). In addition, a dynamic turbidity maximum can be observed that shifts along the estuary over seasonal timescales (indicated by the black ellipses in Fig. 4). During summer, the low river flow facilitates the upstream movement of this dynamic turbidity maximum and in July 2005 it is located near Pauillac (Fig. 4d). In addition, high SSCs occur in the riverine areas, especially in the Garonne river (dotted ellipse in Fig. 4d). Turbidity levels in the rivers decline once fresh water inputs increase, accompanied by the downstream movement of the dynamic turbidity maximum (Fig. 4e). As a result of the ongoing increase in river discharge (which peaks in March 2006), the turbidity maximum continues to migrate towards the mouth of the estuary (Fig. 4f). A comparison between SSC maps from the model (Fig. 4) and satellite data (Fig. 2) shows similar turbidity patterns controlled by variations in river inflow. To further analyze differences and similarities we considered a set of MODIS images taken between 2004 and 2014 and applied Doxaran et al.'s (2009) algorithms to convert these to SSC. We then selected images that were taken close to the moment of high tide in Pauillac and subsequently extracted the averaged surface SSC along the channel for both low (Fig. 5a) and high (Fig. 5b) river discharge conditions. A comparison shows that the model reproduces SSC levels and spatial trends for contrasting river flows.

4.1.2. Time-series

In this section we use the long-term time-series from the MAGEST monitoring network to further test the model and to provide additional evidence of seasonal variation in estuarine physical behaviour. We concentrate on salinity and turbidity measured at two locations: Pauillac and Bordeaux (the other two measuring stations are located further upstream). Fig. 6b shows the simulated and measured salinity at Pauillac, together with the combined river discharge of the Dordogne and Garonne. The seasonal variation is probably the most remarkable. Salinity increases from June 2005 until September 2005, reaching maximum values that exceed 15 psu. The subsequent decrease in salinity is the result of enhanced river flow which tends to flush the saline water from the estuary so that salinity even becomes nil for a short period of time in Pauillac and further upstream (see also Fig. 4c). Simulated salinity corresponds with the measurements which show the same seasonal trend. At the same time, it can be seen that the model generally overpredicts the salinity in July, August and September when river discharge is low and gives an underprediction in February, March and April when river discharge is high. In addition to seasonal fluctuations, both model results and measurements reveal the influence of the spring-neap tidal cycle (shown in Fig. 6a) which modulates salinity patterns. Not surprisingly, variations in salinity throughout a tidal cycle are the largest during spring tides when the tidal range is at its maximum.

Fig. 6c and d show time-series of measured and modelled SSC, also at Pauillac. Although difficult to depict from these figures, intratidal variations are present whereby concentrations of suspended particle matter increase during moments of maximum ebb and flood tidal currents. On the other hand, SSC is low during slack tides, especially during high water slack which lasts longer than low water slack so that more sediment particles can settle. As with salinity, the influence of the spring-neap tidal cycle is clearly portrayed (Fig. 6d). Both measurements and the model show that SSCs are higher during spring tides; this is when tidal currents are stronger and erosion of bottom sediments is enhanced. During neap tide, observed and simulated concentrations may drop below 0.5 g/l (Fig. 6d).

Having considered these intratidal and spring-neap variations, it can be noted that turbidity patterns at Pauillac are rather regular without any seasonal variations caused by river inflow fluctuations. Modelled turbidity values during spring tides reach a maximum value of around 0.5 g/l throughout the entire year. This lack of a seasonal signal at Pauillac is in contrast to turbidity patterns at Bordeaux (detailed below) and is in agreement with measured time-series of SSC (Fig. 6c) and multi-year observations by Sottolichio and Castaing (1999). They discuss SSC measurements from 1984 to 1991 and although their sampling frequency was rather coarse (water samples were taken only three times per year), measurements did cover different flow regimes, suggesting that SSC in the middle estuary has a low sensitivity to river inflow. Further upstream, Sottolichio and Castaing (1999) noticed large variations in turbidity over seasonal scales and river inflow was suggested to be the main factor to control these changes. To assess the importance of a varying river inflow on turbidity in the upper estuary we extracted simulated SSCs at Bordeaux and compared this to measured data (Fig. 7). Indeed, both measurements and the model highlight the response of suspended sediment particles to changes in river inflow. As shown in Fig. 7, the increase in river discharge is followed by a significant decrease in suspended particle matter at Bordeaux. Turbidity is low for several months with SSCs falling below 0.1 g/l until the high discharge period ceases and the normal turbidity regime from before the flood event is restored.

Although the model captures the seasonal trend in sediment dynamics at Bordeaux and reproduces the lack of a seasonal signature at Pauillac, there are some aspects which are less well reproduced. In the model simulation, for example, turbidity at Bordeaux seems to respond slower to increasing river discharge than the observations reveal. It also takes more time before simulated turbidity levels are reaching again their normal levels after the high discharge event. Thus, both model and observations show the response of turbidity to river inflow in the upper estuary, but there is a discrepancy in terms of the timing at which this

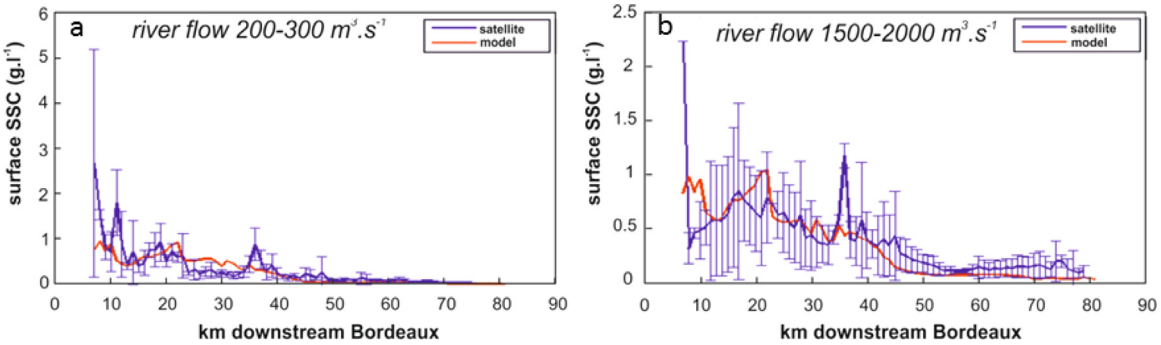

Fig. 5. Comparison between simulated surface SSC and surface SSC retrieved from satellite data along the axis of the channel. a) low river inflow between 200 and 300 m^3/s and b) high river inflow between 1500 and 2000 m^3/s. Satellite images selected for this comparison were taken close to the moment of high tide in Pauillac. Bold blue line indicates average and blue bars indicate minima and maxima of each set of images.

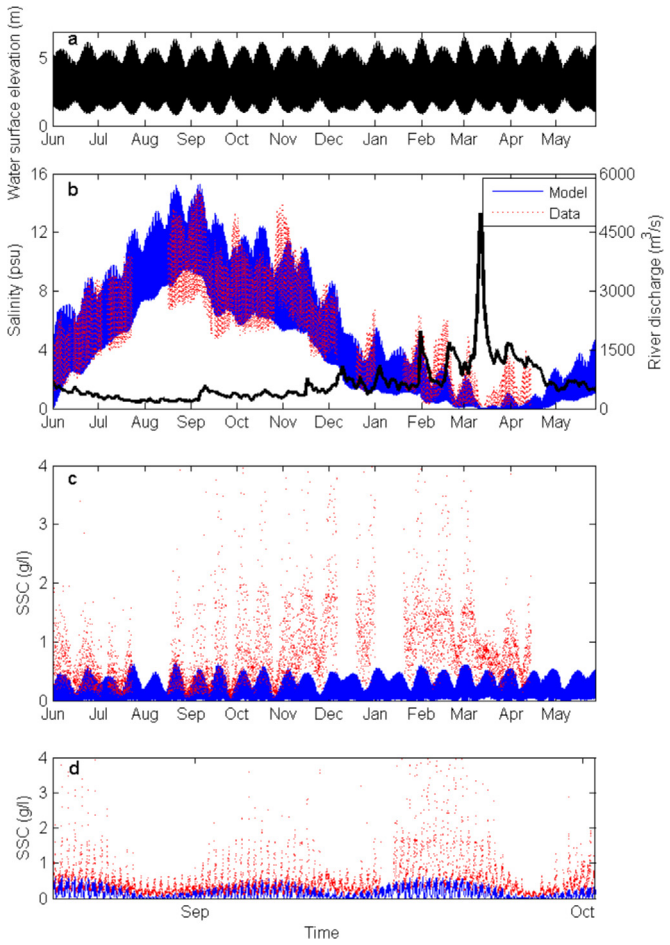

Fig. 6. Time-series of hydro- and sediment dynamics at Pauillac. (a) Simulated water surface elevation. (b) Simulated and measured salinity. The black line represents the combined river discharge of the Dordogne and Garonne. (c) Simulated and measured turbidity from June 2005 until June 2006 and (d) for three spring-neap tidal cycles to provide additional detail.

response occurs. In addition, both at Pauillac and Bordeaux there is a mismatch between the absolute values of modelled and observed turbidity with SSCs generally being underpredicted. The settling velocities could obviously be reduced to obtain a better agreement but, as we will show in Section 4.2.1, this has negative effects on the performance of the model on the long term and on overall sediment budgets. Other potential reasons for data-model inconsistencies will be highlighted in the Discussion (Section 5).

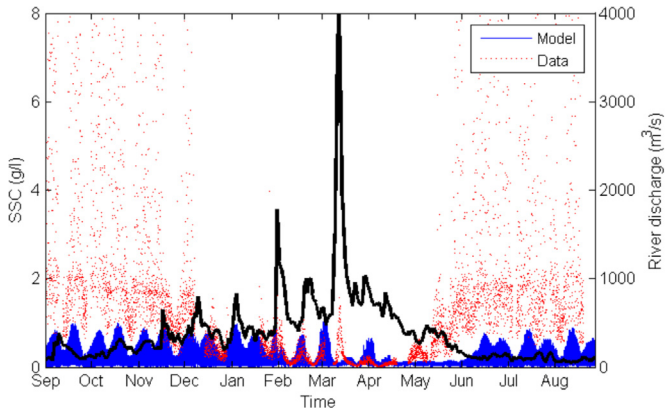

Fig. 7. Simulated and measured turbidity at Bordeaux from September 2005 until September 2006. The black line represents the river discharge of the Garonne.

4.1.3. Sediment budgets

The estuarine sediment budget also illustrates variations in sediment dynamics over various timescales. Fig. 8 shows the simulated balance between the total suspended and deposited sediment load (black lines in Fig. 8d and e), both evaluated over the part of the computational grid that is shown in Fig. 3 (the entire grid extends further offshore as explained in Section 3.2). Overall, the concentration of suspended sediment in the estuarine system is much lower during neap tides than during spring tides. This is conform the turbidity patterns at Pauillac (Fig. 6c and d) and Bordeaux (Fig. 7) and further indicates the importance of relative tidal amplitude and the magnitude of tidal currents on sediment resuspension. Nevertheless, even during neaps a significant proportion of sediment particles remains in suspension which is in contrast to other estuaries, such as the Seine, where most sediment is deposited at neap tide (Le Hir et al., 2001). At the end of the simulation year (June 2006), the amount of suspended sediment is approximately $1.7{\cdot}10^9$ kg while the deposited load amounts to $3.4{\cdot}10^9$ kg, representing a total sediment mass that slightly exceeds 5 million tons. This falls within the estimated range of total sediment mass as described by Allen et al. (1977) and is more than twice the annual input of riverine sediment (Fig. 8c).

Transport of sediment out of the estuarine area and to the offshore (i.e. crossing the grey dashed line in Fig. 3) is only substantial under specific conditions. That is, seaward fluxes mainly occur at spring tides during a period of high river discharge (e.g. at the beginning of the months March, April, May 2006; see Fig. 8f). This suggest that a large river inflow is necessary to force the turbidity maximum to move downstream and this, in combination with spring tides that cause enhanced sediment resuspension, allows for the escape of estuarine sediments to the offshore. This loss of estuarine sediment is accompanied

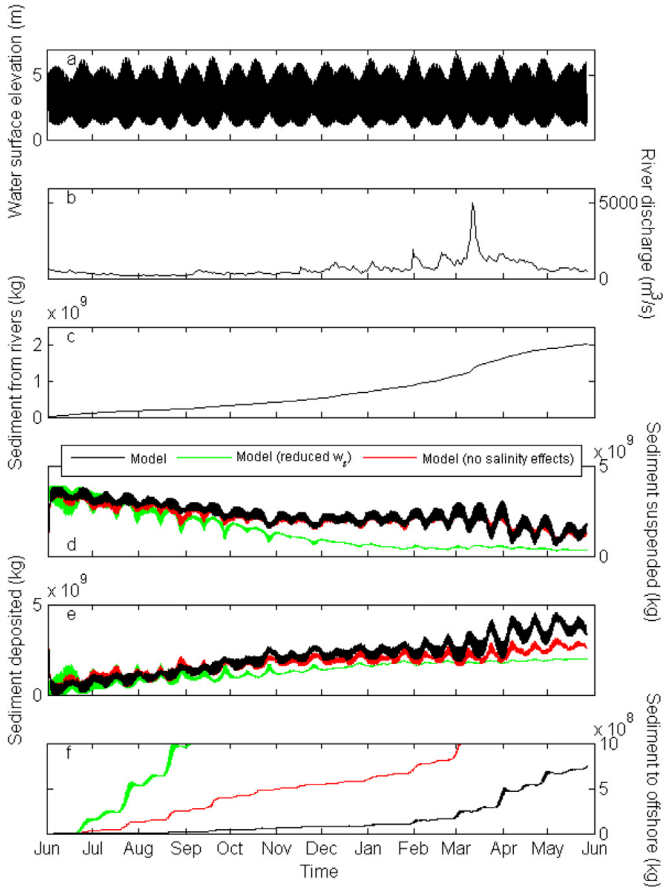

Fig. 8. Modelled sediment balance. (a) Simulated water surface elevation at Pauillac from June 2005 until June 2006. (b) Combined river discharge of the Dordogne and Garonne. (c) Total imports of sediment from the Dordogne and Garonne. (d) Total amount of sediment suspended and (e) total amount of sediment deposited, both evaluated over the part of the computational grid that is shown in Fig. 3. (f) Simulated total amount of sediment leaving the estuarine area (i.e. crossing the grey dashed line in Fig. 3) and escaping to the offshore area. The green lines in (d), (e) and (f) represent the sediment budget for a simulation with lower settling velocity (discussed in Section 4.2.1). Red lines in these subplots represent the sediment budget for a simulation without the effects of salinity on density (discussed in Section 4.2.2). (For interpretation of the references to color in this figure legend, the reader is referred to the web version of this article.).

with a decrease in the overall suspended load (Fig. 8d) and an increase in deposited load (Fig. 8e). Analysis of deposited sediments indicates that this sediment deposition mainly takes place just seaward of Le Verdon in the area near the mouth of the estuary.

4.2. Sensitivity to model settings and parameterizations

In this section we report the results of extra simulations that we performed to investigate model behaviour and performance, and to elucidate the physical processes that govern the formation of the turbidity maximum in the Gironde estuary.

4.2.1. Sensitivity to settling velocity

Sediment settling velocity is one of the principal calibration parameters (French, 2010). As such, in order to reduce the apparent underprediction of SSC by the reference simulation as described in Section 4.1.2, we conducted an additional model run with lower settling velocities (factor 5 reduction in the minimum and maximum settling velocity for the coarse fraction and factor 10 reduction for the fine fraction). As expected, this initially improves model performance by enhancing

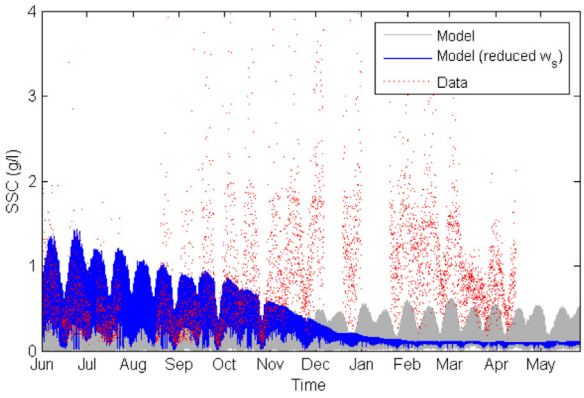

Fig. 9. Data-model comparison for turbidity at Pauillac. Simulation with reduced settling velocities (blue) initially provides a better agreement than reference simulation (grey) but model performance reduces over time. (For interpretation of the references to color in this figure legend, the reader is referred to the web version of this article.).

turbidity levels. At Pauillac, for example, a closer agreement between simulated and measured turbidity is achieved, at least for the first couple of months (Fig. 9). After this initial period, however, model performance drops because of an ongoing decrease in simulated suspended sediment levels. This has been quantified by using the skill score (Eq. (5)) which was computed for four consecutive 3-months periods, as shown in Table 1. For the first quarter of the simulation the skill score amounts to 0.61. This is comparable to the performance of models used in other recent studies on estuarine suspended sediment dynamics (van Maren et al., 2015; Toublanc et al., 2016). The skill score then reduces to a value between 0.3 and 0.4 for subsequent periods. The sediment budget for this simulation indicates that simulated turbidity levels decrease not only at Pauillac, but that the overall amount of suspended matter that is present in the entire estuarine area progressively reduces (green line in Fig. 8d). The loss of suspended particles in the estuary is caused by extensive sediment fluxes to the offshore (Fig. 8f). This in turn is the result of sediment particles staying in suspension more easily such that their transport out of the estuary is being facilitated. Clearly, reducing the settling velocities improves the simulation results on the short term, but at the same time it has negative effects on the longer term performance as it causes an unrealistically high escape of sediment to the offshore.

4.2.2. Sensitivity to density gradients

To explore in more detail the mechanisms that govern the formation and dynamics of the turbidity maximum we performed simulations that did not include the effects of suspended sediment (Fig. 10b) and salinity (Fig. 10c) on density and compared these to the reference simulation (Fig. 10a). Both suspended particle matter and salinity contribute to the density of water and, as such, they play a role in enhancing stratification which in turn induces turbulence damping and residual circulation. Ignoring the effect of suspended sediment mainly changes the vertical distribution of turbidity levels (compare Fig. 10a and b). Suspended particles can penetrate further up in the water column as turbulence damping is not as significant. Especially at the water surface there is a

Table 1
Skill scores calculated for simulated turbidity at Pauillac with reduced settling velocities (see Fig. 9).

	Skill score
June 2005 – August 2005	0.61
September 2005 – November 2005	0.35
December 2005 – February 2006	0.37
March 2006 – May 2006	0.32

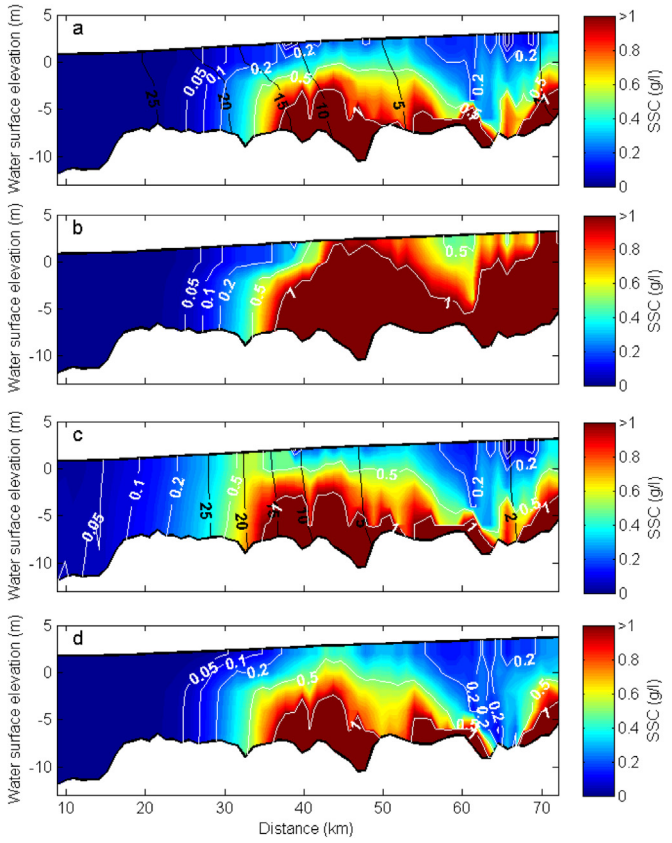

Fig. 10. Turbidity distributions along the estuary modelled for low river discharge at low tide during spring conditions. See Fig. 3 for location of transect. Distance is measured from Le Verdon. (a) Scenario including effects of SSC and salinity on fluid density. Alternative distributions simulated without the effects of (b) SSC or (c) salinity on density. (d) Simulated turbidity distribution including a 1.0 m sea level rise. Black contour lines in (a) and (c) represent simulated isohalines.

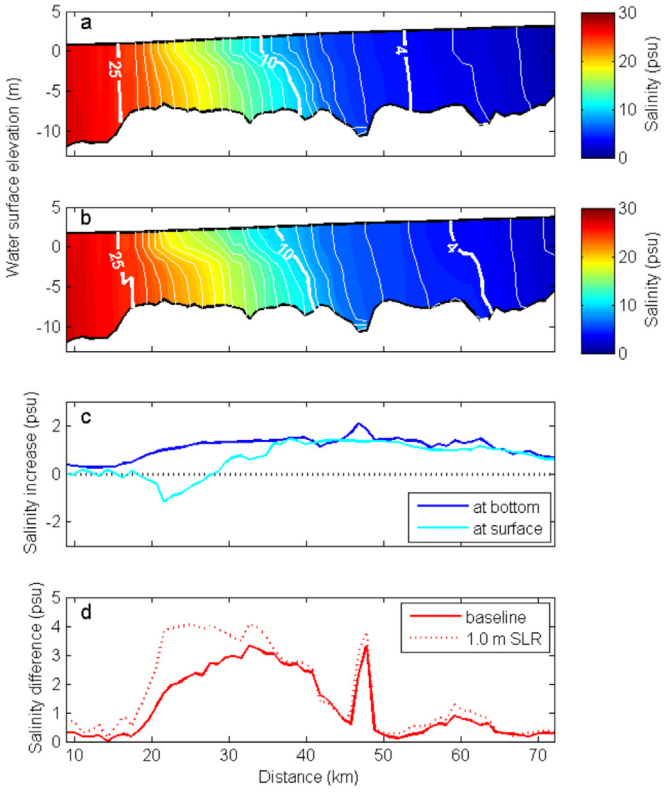

Fig. 11. Sea level rise effects on salinity patterns. (a) Simulated salinity distribution during low river discharge. Salinity distribution is shown at low tide during spring conditions. (b) Corresponding salinity distribution for a 1.0 m sea level rise. (c) Sea level rise driven increase in salinity (i.e. sea level rise value minus baseline value), both at bottom and surface. (d) Effect of sea level rise on stratification (computed as salinity difference between bottom and surface).

clear increase in SSC with values reaching up to 1 g/l. When the effect of salinity on density is not included, it can be seen that the downstream limit of the turbidity maximum is less sharp (compare Fig. 10a and c). This highlights the influence of density-driven residual circulation on the stability of the estuarine turbidity maximum and on the seaward dispersion of suspended sediment. The latter is also exemplified by the sediment budget, which shows a larger escape of sediment to the offshore when density gradients from salinity are not included (red line in Fig. 8f). These findings confirm the main role of tidal asymmetry on turbidity maximum formation as hypothesized by Sottolichio et al. (2001). Density gradients play a secondary role by maintaining a stable mass of suspended sediment within the estuary.

4.3. Sensitivity to sea level rise

In addition to seasonal fluctuations controlled by variation in river inflow, changes in downstream boundary conditions associated with sea level rise are also expected to have a large impact on estuarine dynamics (Mitchell and Uncles, 2013). A key consequence of a rising sea level is the possibility of enhanced salinity intrusion (FitzGerald et al., 2008). An additional model run was conducted with a sea level rise of 1.0 m, such that potential implications for hydro- and sediment dynamics in the Gironde estuary could be explored. A 1.0 m rise is within the range of scenarios that has been used by other recent studies looking at salt intrusion (Rice et al., 2012; Chua and Xu, 2014; Prandle and Lane, 2015; Yang et al., 2015). Fig. 11 shows the simulated salinity distributions for both the reference simulation and the simulation that includes sea level rise. The upstream movement of the isohalines is most profound in the middle estuary. The 4 psu isohaline, for example, migrates about 10 km at the bottom and 6 km at the surface. In this part of the estuary the isohalines are however widely spaced such that the absolute increase in salinity does not exceed far above 1 psu (Fig. 11c). Further downstream, the isohalines move less in response to sea level rise. This is exemplified by the 10 and 25 psu isohalines which have somewhat retained their original location. Interestingly, salinity at the surface actually decreases for a small section in the lower part of the estuary (negative change for surface salinity at around 22 km in Fig. 11c). At the bottom, salinity consistently increases such that stratification at this location is enhanced and the difference between bottom and surface salinity increases from 2 to 4 psu (Fig. 11d). This enhanced stratification suggests that the gravitational circulation is strengthened by the rise in sea level.

Sea level rise effects on turbidity maximum properties are less obvious. Along-estuary SSC profiles indicate that the geometry and intensity of the turbidity maximum remain essentially unaltered (compare Fig. 10a and d) and spatial SSC distributions before and after sea level rise are also comparable (Fig. 12). However, sea level rise can locally influence resuspension of bottom sediment in response to changes in the characteristics of the tide (Fig. 13). Effects are most strongly manifested in the upper estuary where the tidal range increases about 10–30% (e.g. Fig. 13c). Here the tidal current is strengthened and it is mainly the peak flood current that increases in magnitude (Fig. 13f). This causes enhanced levels of suspended particle matter, especially during the flood phase (Fig. 13i). In the middle and lower estuary, changes in the tidal range are smaller (Fig. 13b) or almost null (Fig. 13a) and current velocities remain similar (Fig. 13d and e). A clear signature of sea level rise on simulated turbidity levels is therefore less

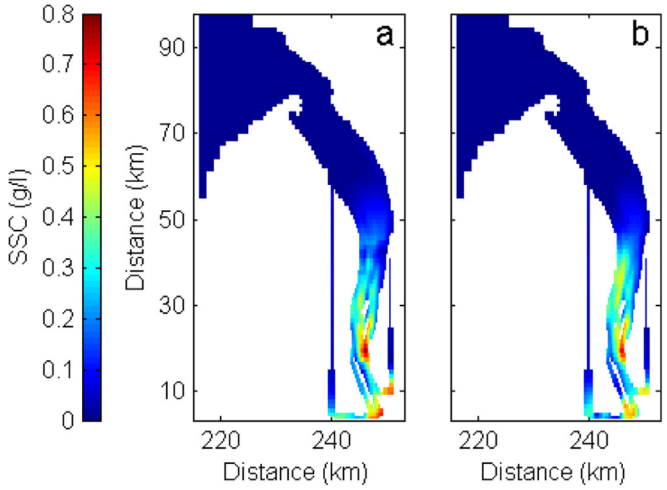

Fig. 12. Simulated turbidity fields before (a) and after (b) a 1.0 m sea level rise.

obvious (Fig. 13g and h).

To further analyze sea level rise effects on tidal characteristics we conducted a harmonic analysis for different locations within the estuary. Close to Le Verdon (represented by the pink dot in Fig. 14a), sea level rise neither influences the amplitude of the M_2 nor M_4 tidal component. However, when moving upstream to the middle estuary, an increase in the M_2 tidal amplitude due to sea level rise can readily be observed (e.g. at Pauillac; blue dot in Fig. 14a). The largest change occurs in the upper estuary where the amplitude of the M_2 component increases with approximately 0.45 m. This is in the region where the tidal wave is generally being damped due to the shallow bathymetry. The M_4 tidal amplitude also increases but less substantially and only in the upper estuary. M_2 and M_4 velocity amplitude also increases in the upstream region (Fig. 14b), consistent with strengthening of the tidal current as mentioned above (Fig. 13f). Regardless of the changes in the amplitude of both the water level and the velocity, sea level rise generally does not have an effect on the tidal distortion factor defined by $M_{4amplitude}$ / $M_{2amplitude}$ (black lines in Fig. 14a and b). Sea level rise neither influences the tidal dominance factor which takes into account the phasing of the tidal components (Fig. 14c and d). The tidal dominance factor indicates whether flood-dominant or ebb-dominant conditions prevail. For the Gironde estuary, the middle and upper regions are clearly flood-dominant, both before and after sea level rise.

5. Discussion

5.1. Advantages of yearly simulations and model limitations

The modelling results presented here show some of the benefits of simulations over seasonal timescales, in contrast to shorter term simulations in the order of individual tidal cycles to weeks which are more commonly conducted (see also Mitchell and Uncles, 2013). Yearly simulations allow for a more comprehensive assessment of seasonal processes such as the movement of the turbidity maximum in response

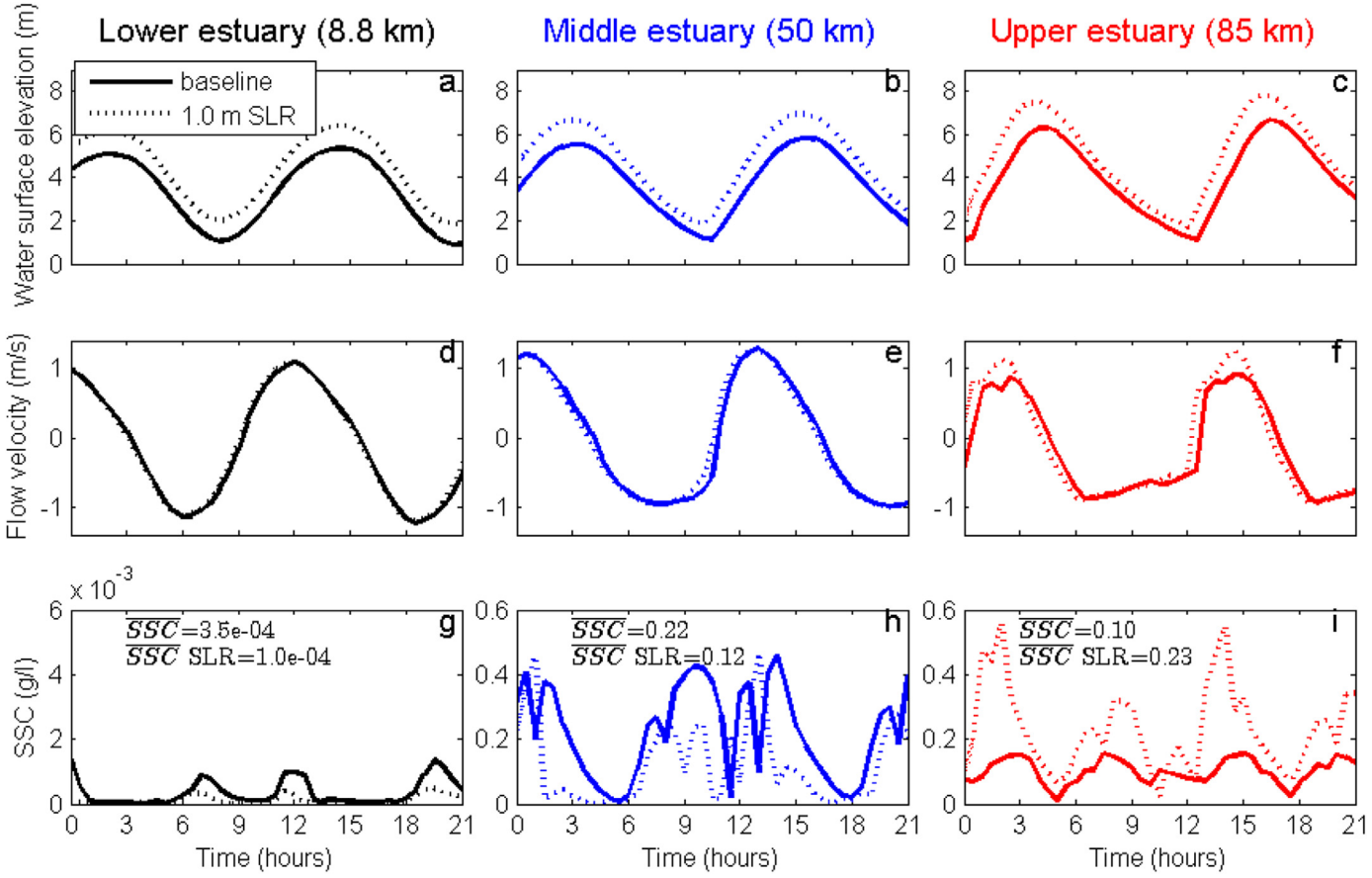

Fig. 13. Sea level rise effects on tidal propagation and SSC patterns for the lower, middle and upper estuary. Simulated temporal evolution of (a, b, c) water surface elevation (d, e, f) flow velocity and (g, h, i) SSC before (solid lines) and after (dotted lines) a rise in mean water level of 1.0 m. The coloured dots in Fig. 3 indicate the locations for which the time-series have been extracted. Subplots (g), (h) and (i) include information on time-averaged SSC indicating an increase in turbidity levels in the upper estuary. Turbidity levels in the middle estuary are decreasing but this is mainly because SSC is extracted at the water surface; sea level rise causes a larger water depth such that the number of sediment particles reaching the surface is reduced.

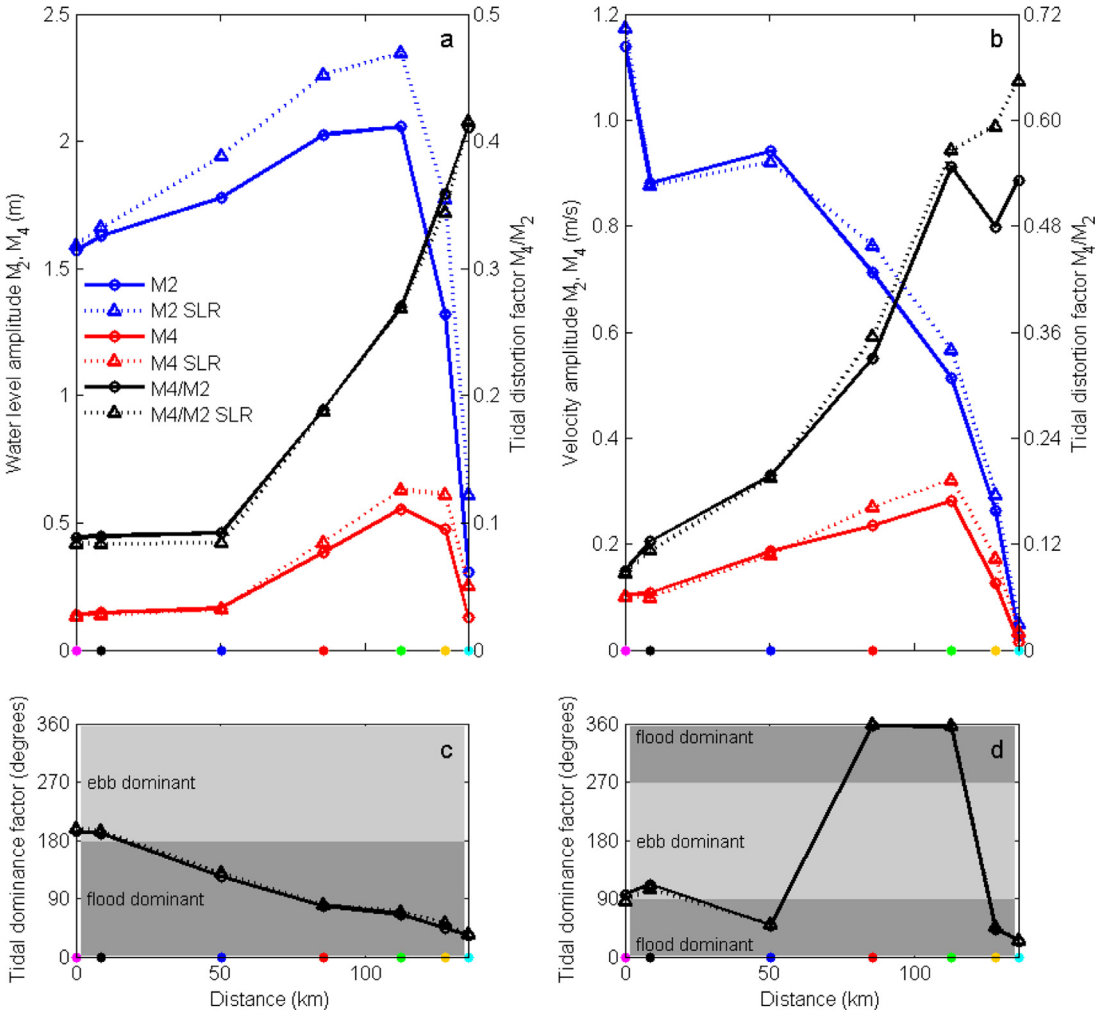

Fig. 14. Sea level rise effects on tidal characteristics. (a) M_2 water level amplitude, M_4 water level amplitude, and tidal distortion factor $M_{4amplitude}$ / $M_{2amplitude}$. Solid lines indicate present situation and dotted lines indicate 1.0 m sea level rise scenario. (b) M_2 velocity amplitude, M_4 velocity amplitude, and tidal distortion factor $M_{4amplitude}$ / $M_{2amplitude}$. Tidal dominance factor $2M_{2phase}$-M_{4phase} for (c) water level and (d) velocity. The coloured dots on the x-axes and in Fig. 3 indicate the locations for which the tidal harmonic analysis was conducted.

to changing river inflow. The drop in turbidity levels caused by a river flood, for example, and the subsequent increase in turbidity after the high discharge event has passed are important dynamics that can only be assessed in detail when simulations over seasonal timescales are conducted. This includes the associated timing of these events and potential hysteresis effects in SSC patterns as observed for the upper reaches of the Gironde estuary (Fig. 7).

For the Gironde estuary we show here that tidal asymmetry is the primary forcing driving the formation of a turbidity maximum. Still, model simulations of only a few tidal cycles could have shown that a turbidity maximum forms without the consideration of density gradients. Yearly simulations, however, provide additional insights by showing that density effects play an important role in maintaining the stability of the turbidity maximum and without these effects a large proportion of the fine sediment escapes to the offshore. Toublanc et al. (2016) recently described a similar finding for the Charente estuary which is also a macrotidal system located just north of the Gironde estuary but with a significantly smaller riverine input. Based on model runs they concluded as well that density gradients play an important role in ensuring a sharper downstream limit of the suspended sedimentary mass, preventing the massive export of sediments. This is in turn consistent with some earlier modelling efforts carried out by Brenon and Le Hir (1999) who also pointed out the dominant role of tidal pumping for the Seine estuary (north-west coast of France). Thus, tidal asymmetry as the main driver with a secondary role for density effects seems to be a consistent feature, at least for the macrotidal estuaries along the French Atlantic coast.

Finally, the yearly simulations presented here further highlight the need to evaluate model behaviour over different timescales. One of the parameters that is commonly tuned to improve model results is the settling velocity of sediment particles and adjusting this velocity indeed also enhanced model performance in our study (Fig. 9). At least for the first couple of months, as discussed, but after that the excessive and ongoing escape of sediment to the offshore leads to incorrect model behaviour as the turbidity in the estuary becomes unrealistically low. This hinders the process of defining optimum values for the settling velocity. It also implies that sediment fluxes at the mouth should be one of the criteria for model calibration. Calibrating models of estuarine sediment dynamics is further complicated by the parametric complexity involved in estuarine sediment modelling (French, 2010; Payo et al., 2016). The process of particle settling in particular is difficult to represent as the parameterization is dependent on a range of complex cohesive processes (Amoudry and Souza, 2011; Wang et al., 2012). In addition to hindered settling and flocculation, factors like turbulence and salinity gradients are all expected to play a role (Priya et al., 2015). As such, large spatial variations in settling velocities are to be expected and adopting more accurate representations will inherently enhance model performance. However, the data to constrain these

parameterizations for the Gironde estuary are unavailable and difficult to obtain and this remains a key area of future research.

Although simulations in the order of 1 year or more provide advantages, these types of models are computationally intensive and it requires certain compromises in terms of model set-up to keep the running time manageable. We here used an irregular grid to keep the number of computational points to a minimum while obtaining a fine resolution in the areas of interest. Still, the width of the rivers in the upper reaches of the estuary is only resolved by 1–3 grid cells and a higher resolution will most likely improve model results in these specific areas. Measurements of SSC at Bordeaux, for example, were obtained in the proximity of existing mudflats. Although limited in size, these mudflats might influence local sedimentary processes that are not resolved due to the used model grid. The grid resolution, however, was mainly adjusted to match the focus of this study, which is on enhancing our understanding of the larger scale hydro- and sediment dynamics, specifically the spatial patterns in SSC and the geometries of turbidity maxima, seasonal patterns driven by river inflow, sediment budgets, and potential trends in salinity and turbidity caused by sea level rise. Another way forward to overcome the drawback of high computational cost is to combine numerical models with the use of idealized models to benefit from the strengths of both types (Schuttelaars et al., 2013).

5.2. Future changes in river discharge and sea level rise

Historical records show that the annual discharge of the Garonne and Dordogne rivers has been decreasing, flood events are increasingly scarce and drought periods are becoming more durable (Jalón-Rojas et al., 2015). How river inflow will change in the future is still uncertain, but based on climate change scenarios and streamflow simulations it is the expectation that average discharges will continue to decrease (Boé et al., 2009; Alfieri et al., 2015). Although the current study does not address multi-decadal changes in river inflow, the simulations presented here do highlight that estuarine hydro- and sediment dynamics are highly sensitive to changes in fluvial discharge. Fig. 15 summarizes this dominating role of river inflow by showing the dependency of salinity intrusion and turbidity maximum location on river discharge. Seasonal variations in river conditions drive a displacement of the salinity front (0.5 psu isohaline) that exceeds 40 km (Fig. 15a) and the along-estuary shift of the turbidity maximum is in the same order of magnitude (Fig. 15b). As an indication of decadal changes in estuarine dynamics, we included in Fig. 15 the mean annual discharge of the periods 1960s-1980s (1000 m^3/s) and 2005–2014 (680 m^3/s) (Jalón-Rojas et al., 2015), together with a rough estimate of future discharge. According to projections, it is plausible that the mean annual discharge will drop further to 500 m^3/s or lower within this century (Boé et al., 2009), which would force a further upstream movement of the salinity front and turbidity maximum (Fig. 15). Clearly, these types of insights obtained from seasonal variations in hydrosedimentary dynamics can be valuable for anticipating impacts of future changes in river inflow.

Impacts of sea level rise have been more explicitly assessed. As pointed out, elevated salinity levels in the middle estuary is one of the key consequences, and the simulated effects are in the same order as those of some other large estuarine systems. Hong and Shen (2012), for example, conducted model runs to explore sea level rise effects for the Chesapeake Bay. They simulated a salinity increase of around 1–2 ppt along the main axes of the Bay for a sea level rise of 1.0 m and a typical dry year. This is comparable to salinity increases reported here (Fig. 11c). For the Chesapeake Bay salinity changes include an upstream movement of the salinity front (0.5 psu isohaline) of more than 10 km (Hong and Shen, 2012). This, however, is in contrast with our findings for the Gironde where the effects of sea level rise on the location of the salinity front (indicated by asterisks in Fig. 15a) are almost negligible and overshadowed by river discharge effects. Other hydrodynamic sea level rise impacts reported by Hong and Shen (2012) include enhanced stratification, increase in the tidal amplitude, and an earlier arrival of low and high water, all consistent with our findings for the Gironde estuary.

Modelling studies assessing the implications of sea level rise on the dynamics of turbidity maxima are less abundant. The general consensus is that sea level rise pushes the turbidity maximum further upstream (Robins et al., 2016). For the Gironde we observe that sea level rise effects are of minor importance in comparison to variations caused by changes in river inflow (Fig. 15b). In addition to the location of the turbidity maximum, it was observed that its geometry and intensity were neither affected by a rising sea level (Fig. 10a and d). A potential explanation may be found in the tidal characteristics of the estuarine area where the turbidity maximum predominantly occurs. Model simulations indicate that the depth of the lower and middle estuary is sufficiently large such that tidal wave damping is limited. As a consequence, sea level rise does not influence tidal propagation or velocity patterns in a large proportion of the estuary. As the location of the salinity front remains relatively stable too this suggests that turbidity

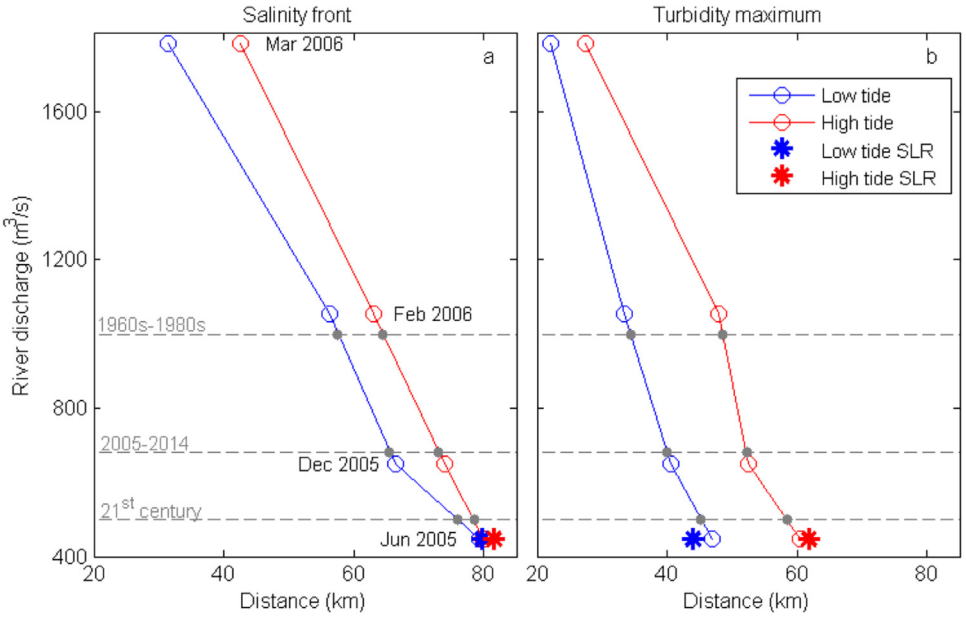

Fig. 15. Effects of river discharge and sea level rise on location of (a) salinity front (0.5 psu isohaline) and (b) turbidity maximum. Distance is measured from Le Verdon. As an indication of decadal changes, the mean annual discharge of the periods 1960s-1980s (1000 m^3/s) and 2005–2014 (680 m^3/s) (Jalón-Rojas et al., 2015) are shown, together with a rough estimate of future discharge (500 m^3/s) within the 21st century.

maximum characteristics are relatively insensitive to a rising sea level.

Finally, our sea level rise simulations also compare to systems which have been subject to channel deepening as a result of dredging. The Ems estuary is such a system that has been deepened during the past decades and studies have shown how this has led to tidal amplification with tides penetrating deeper into the estuary and significant increases in turbidity levels in the upstream tidal river (Chernetsky et al., 2010; Winterwerp and Wang, 2013; de Jonge et al., 2014; van Maren et al., 2015). These effects are comparable with those of the Gironde estuary under a rising sea level as the simulations presented here suggest an increase in the tidal range, stronger tidal currents and rising SSC levels in the upper estuary. For the Ems estuary this has resulted in hyper-turbid conditions with negative implications for light penetration, oxygen levels and primary productivity (Talke et al., 2009b; de Jonge et al., 2014). The navigation channels of the Gironde estuary are regularly dredged as well, but possible effects on turbidity levels are yet to be fully explored. As sea level rise could potentially exacerbate the effects of dredging this clearly highlights the need to study the risk of a regime shift to hyper-turbidity in the upper reaches of the Gironde estuary. The development of hyper-turbid conditions, however, is a highly complex process governed by multiple operating feedbacks and, as such, this remains a key area of future research, especially considering the large environmental impacts involved.

6. Conclusions

A numerical model was used to identify the response of hydro-sedimentary dynamics in the Gironde estuary to variations in river inflow and sea level rise. Comparisons with satellite imagery and time-series of measured salinity and SSC show that the model reproduces observed seasonal trends. In addition, numerical experiments were undertaken to improve understanding of the governing mechanisms responsible for the formation of the turbidity maximum. The main conclusions can be summarised as follows:

- Salt water intrusion is strongly dependent on river discharge and the migration of the salinity front in response to seasonal variations in river inflow is in the order of 40 km.
- The model is capable of reproducing the formation of a well-developed turbidity maximum which shifts along the estuary over seasonal timescales and a secondary turbidity maximum which is more stable.
- SSC patterns at Bordeaux (upper estuary) are controlled by seasonal fluctuations while turbidity levels at Pauillac (middle estuary) prove to be insensitive to river flow variations.
- Sediment export mainly occurs during periods of high river discharge which forces the turbidity maximum to move downstream in combination with spring tides which enhance sediment resuspension.
- Tidal asymmetry is the main driver of turbidity maximum formation. Density gradients play a secondary role by maintaining a stable mass of suspended sediment within the estuary and limiting seaward dispersion.
- Simply adjusting settling velocities to reduce the underprediction of SSC improves model skill on the short term, but leads to unrealistically high escape of sediment to the offshore and depletion of the estuarine sediment mass.
- Sea level rise increases salinity levels in the middle estuary by approximately 1 psu. The location of the salinity front remains relatively stable. In the upper estuary, sea level rise causes tidal amplification, strengthening of tidal currents and enhanced SSC levels.
- The location, geometry and intensity of the turbidity maximum remain essentially unaltered under sea level rise. Decadal changes in river inflow are suggested to have a larger effect on location than rising water levels.

A key aspect of future research involves exploring the risk of a regime shift to hyper-turbid conditions in the upper reaches of the Gironde estuary. Sea level rise could exacerbate the effects of ongoing dredging by amplifying the tide and driving a further increase in turbidity levels. This potentially has large consequences for the environmental quality of the estuary.

Acknowledgements

This work was funded by the Agence de l'Eau Adour Garonne (AEAG) and the Conseil Régional d'Aquitaine (CRA). We thank Pierre Le Hir for discussions on model application and Maarten Kleinhans for comments on an earlier version of the manuscript. The MAGEST Consortium is acknowledged for providing field data on salinity and turbidity. MODIS remote sensing data was processed in the framework of the CNES RIVERCOLOR Project with the valuable contribution of Virginie Lafon (I-Sea) and Lydia Ouamar. We thank the reviewers for providing detailed and constructive feedback.

References

Alfieri, L., Burek, P., Feyen, L., Forzieri, G., 2015. Global warming increases the frequency of river floods in Europe. Hydrol. Earth Syst. Sci. 19, 2247–2260. http://dx.doi.org/10.5194/hess-19-2247-2015.

Allen, G.P., 1972. Etude des processus sedimentaires dans l'estuaire de la Gironde (Ph.D. thesis). University of Bordeaux, pp. 314.

Allen, G.P., Sauzay, G., Castaing, P., Jouanneau, J.M., 1977. Transport and deposition of suspended sediment in the Gironde estuary, France. In: Wiley, M. (Ed.), Estuarine Processes 2. Academic Press, New Yoirk, pp. 63–81.

Allen, G.P., Salomon, J.C., Bassoullet, P., Du Penhoat, Y., De Grandpré, C., 1980. Effects of tides on mixing and suspended sediment transport in macrotidal estuaries. Sediment. Geol. 26, 69–90.

Amoudry, L.O., Souza, A.J., 2011. Deterministic coastal morphological and sediment transport modeling: a review and discussion. Rev. Geophys. 49. http://dx.doi.org/10.1029/2010RG000341. (RG).

Boé, J., Terray, L., Martin, E., Habets, F., 2009. Projected changes in components of the hydrological cycle in French river basins during the 21st century. Water Resour. Res. 45. http://dx.doi.org/10.1029/2008WR007437.

Brenon, I., Le Hir, P., 1999. Modelling the turbidity maximum in the Seine estuary (France): identification of formation processes. Estuar. Coast. Shelf Sci. 49, 525–544.

Burchard, H., Bolding, K., Villarreal, M.R., 2004. Three-dimensional modelling of estuarine turbidity maxima in a tidal estuary. Ocean Dyn. 54, 250–265.

Cancino, L., Neves, R., 1999. Hydrodynamic and sediment suspension modelling in estuarine systems. Part II: application to the Western Scheldt and Gironde estuaries. J. Mar. Syst. 22, 117–131.

Castaing, P., Allen, G.P., 1981. Mechanisms controlling seaward escape of suspended sediment from the Gironde: a macrotidal estuary in France. Mar. Geol. 40, 101–118.

Chernetsky, A.S., Schuttelaars, H.M., Talke, S.A., 2010. The effect of tidal asymmetry and temporal settling lag on sediment trapping in tidal estuaries. Ocean Dyn. 60, 1219–1241.

Chua, V.P., Xu, M., 2014. Impacts of sea-level rise on estuarine circulation: an idealized estuary and San Francisco Bay. J. Mar. Syst. 139, 58–67.

Coynel, A., Schäfer, J., Hurtrez, J.-E., Dumas, J., Etcheber, H., Blanc, G., 2004. Sampling frequency and accuracy of SPM flux estimates in two contrasted drainage basins. Sci. Total Environ. 330, 233–247.

Cugier, P., Le Hir, P., 2002. Development of a 3D hydrodynamic model for coastal ecosystem modelling. Application to the plume of the Seine river (France). Estuar. Coast. Shelf Sci. 55, 673–695.

de Jonge, V.N., Schuttelaars, H.M., van Beusekom, J.E., Talke, S.A., de Swart, H.E., 2014. The influence of channel deepening on estuarine turbidity levels and dynamics, as exemplified by the Ems estuary. Estuar. Coast. Shelf Sci. 139, 46–59.

Doxaran, D., Froidefond, J.M., Castaing, P., Babin, M., 2009. Dynamics of the turbidity maximum zone in a macrotidal estuary (the Gironde, France): observations from field and MODIS satellite data. Estuar. Coast. Shelf Sci. 81, 321–332.

Dyer, K.R., 1986. Coastal and Estuarine Sediments Dynamics. John Wiley & Sons Ltd, Chichester, UK, pp. 342.

Dyer, K.R., 1988. Fine sediment particle transport in estuaries. In: Dronkers, J., van Leussen, W. (Eds.), Physical Processes in Estuaries. Springer, Berlin Heidelberg, pp. 295–310.

Dyer, K.R., 1997. Estuaries: A Physical Introduction, 2nd edition. John Wiley & Sons Ltd, Chichester, UK, pp. 195.

FitzGerald, D.M., Fenster, M.S., Argow, B.A., Buynevich, I.V., 2008. Coastal impacts due to sea-level rise. Annu. Rev. Earth Planet. Sci. 36, 601–647.

French, J.R., 2010. Critical perspectives on the evaluation and optimization of complex numerical models of estuary hydrodynamics and sediment dynamics. Earth Surf. Process. Landf. 35, 174–189.

Geyer, R., 1993. The importance of suppression of turbulence by stratification on the estuarine turbidity maximum. Estuaries 16, 113–125.

Hong, B., Shen, J., 2012. Responses of estuarine salinity and transport processes to

potential future sea-level rise in the Chesapeake Bay. Estuar. Coast. Shelf Sci. 104, 33–45.
Huijts, K.M.H., Schuttelaars, H.M., de Swart, H.E., Valle-Levinson, A., 2006. Lateral entrapment of sediment in tidal estuaries: an idealized model study. J. Geophys. Res. 111. http://dx.doi.org/10.1029/2006JC003615.
Huijts, K.M.H., Schuttelaars, H.M., de Swart, H.E., Friedrichs, C.T., 2009. Analytical study of the transverse distribution of along-channel and transverse residual flows in tidal estuaries. Cont. Shelf Res. 29, 89–100.
Jalón-Rojas, I., Schmidt, S., Sottolichio, A., 2015. Turbidity in the fluvial Gironde Estuary (southwest France) based on 10-year continuous monitoring: sensitivity to hydrological conditions. Hydrol. Earth Syst. Sci. 19, 2805–2819.
Jay, D.A., Musiak, J.D., 1994. Particle trapping in estuarine tidal flows. J. Geophys. Res. 99, 20445–20461.
Jouanneau, J.M., 1979. Evaluation du volume et de la masse des matieres en suspension dans le systeme bouchon vaseuxcreme de vase de la Gironde. Bull. Inst. Geol. Bassin Aquitaine 25, 111–120.
Jouanneau, J.M., Latouche, C., 1981. The Gironde estuary. In: Füchtbauer, H., Lisitzy, A.P., Millerman, J.D., Seibold, E. (Eds.), Contributions to Sedimentology. E. Schweirzerbat'sche Verglagsbuchhandlung, Stuttgart, pp. 1–115.
Krone, R.B., 1962. Flume Studies of the Transport of Sediment in Estuarial Shoaling Processes, Technical Report of Hydraulic Engineering Laboratory. University of California, Berkeley, pp. 110.
Lajaunie-Salla, K., Wild-Allen, K., Sottolichio, A., Thouvenin, B., Litrico, X., Abril, G., 2017. Impact of urban effluents on summer hypoxia in the highly turbid Gironde Estuary, applying a 3D model coupling hydrodynamics, sediment transport and biogeochemical processes. J. Mar. Syst. 174, 89–105.
Le Cann, B., 1990. Barotropic tidal dynamics of the Bay of Biscay shelf: observations, numerical modelling and physical interpretation. Cont. Shelf Res. 10, 723–758.
Le Hir, P., Karlikow, N., 1992. Sediment transport modelling in a macrotidal estuary: do we need to account for consolidation processes? In: Proceedings of the 23rd International Conference on Coastal Engineering, Venice.
Le Hir, P., Ficht, A., Jacinto, R.S., Lesueur, P., Dupont, J.-P., Lafite, R., Brenon, I., Thouvenin, B., Cugier, P., 2001. Fine sediment transport and accumulations at the mouth of the Seine estuary (France). Estuaries 24, 950–963.
Le Normant, C., 2000. Three-dimensional modelling of cohesive sediment transport in the Loire estuary. Hydrol. Process. 14, 2231–2243.
Li, M., Zhong, L., Boicourt, W.C., 2005. Simulations of Chesapeake Bay estuary: sensitivity to turbulence mixing parameterizations and comparison with observations. J. Geophys. Res.: Oceans 110, C12004. http://dx.doi.org/10.1029/2004JC002585.
Lin, J., Kuo, A.Y., 2003. A model study of turbidity maxima in the York River Estuary, Virginia. Estuar. Coasts 26, 1269–1280.
Mitchell, S.B., Uncles, R.J., 2013. Estuarine sediments in macrotidal estuaries: future research requirements and management challenges. Ocean Coast. Manag. 79, 97–100.
Murray, A.B., 2003. Contrasting the goals, strategies, and predictions associated with simplified numerical models and detailed simulations. In: Wilcock, P.R., Iverson, R. M. (eds), Prediction in Geomorphology, Washington D.C., pp. 151–165.
Park, K., Wang, H.V., Kim, S.-C., Oh, J.-H., 2008. A model study of the estuarine turbidity maximum along the main channel of the Le Normant, C., 2000. three-dimensional modelling of cohesive sediment transport in the Loire estuary. Hydrol. Process. 14, 2231–2243.
Partheniades, E., 1965. Erosion and deposition of cohesive soils. J. Hydraul. Div. 91, 105–139.
Payo, A., Hall, J.W., French, J., Sutherland, J., van Maanen, B., Nicholls, R.J., Reeve, D.E., 2016. Causal loop analysis of coastal geomorphological systems. Geomorphology 256, 36–48.
Postma, H., 1967. Sediment transport and sedimentation in the estuarine environment. In: Lauff, G.H. (Ed.), Estuaries. American Association for the Advancement of Science, Washington, D.C., pp. 158–179.
Prandle, D., Lane, A., 2015. Sensitivity of estuaries to sea level rise: vulnerability indices. Estuar. Coast. Shelf Sci. 160, 60–68.
Priya, K.L., Jegathambal, P., James, E.J., 2015. On the factors affecting the settling velocity of fine suspended sediments in a shallow estuary. J. Oceanogr. 71, 163–175.
Rice, K.C., Hong, B., Shen, J., 2012. Assessment of salinity intrusion in the James and Chickahominy Rivers as a result of simulated sea-level rise in Chesapeake Bay, East Coast, USA. J. Environ. Manag. 111, 61–69.
Robins, P.E., Skov, M.W., Lewis, M.J., Giménez, L., Davies, A.G., Malham, S.K., Neill, S.P., McDonald, J.E., Whitton, T.A., Jackson, S.E., Jago, C.F., 2016. Impact of climate change on UK estuaries: a review of past trends and potential projections. Estuar. Coast. Shelf Sci. 169, 119–135.
Schäfer, J., Blanc, G., Lapaquellerie, Y., Maillet, N., Maneux, E., Etcheber, H., 2002. Ten-year observation of the Gironde tributary fluvial system: fluxes of suspended matter, particulate organic carbon and cadmium. Mar. Chem. 79, 229–242.
Schuttelaars, H.M., de Jonge, V.N., Chernetsky, A., 2013. Improving the predictive power when modelling physical effects of human interventions in estuarine systems. Ocean Coast. Manag. 79, 70–82.
Simpson, J.H., Brown, J., Matthews, J., Allen, G., 1990. Tidal Straining, Density Currents, and Stirring in the Control of Estuarine Stratification. Estuaries 13, 125–132.
Sottolichio, A., Castaing, P., 1999. A synthesis on seasonal dynamics of highly-concentrated structures in the Gironde estuary. Comptes Rendus de l'Académie des Sciences-Series IIA-Earth Planet. Sci. 329, 795–800.
Sottolichio, A., Le Hir, P., Castaing, P., 2001. Modeling mechanisms for the turbidity maximum stability in the Gironde estuary, France. In: McAnally, W.H., Mehta, A.J. (Eds.), Coastal and Estuarine Fine Sediment Processes. Elsevier, Amsterdam, pp. 373–386.
Sottolichio, A., Castaing, P., Etcheber, H., Maneux, E., Schmeltz, M., Schmidt, S., 2011. Observations of suspended sediment dynamics in a highly turbid macrotidal estuary, derived from continuous monitoring. J. Coast. Res. SI 64, 1579–1583.
Talke, S.A., de Swart, H.E., Schuttelaars, H.M., 2009a. Feedback between residual circulations and sediment distribution in highly turbid estuaries: an analytical model. Cont. Shelf Res. 29, 119–135.
Talke, S.A., de Swart, H.E., de Jonge, V.N., 2009b. An idealized model and systematic process study of oxygen depletion in highly turbid estuaries. Estuar. Coasts 32, 602–620.
Thouvenin, B., Gonzalez, J.L., Chiffoleau, J.F., Boutier, B., Le Hir, P., 2007. Modelling Pb and Cd dynamics in the Seine estuary. Hydrobiologia 588, 109–124.
Toublanc, F., Brenon, I., Coulombier, T., 2016. Formation and structure of the turbidity maximum in the macrotidal Charente estuary (France): influence of fluvial and tidal forcing. Estuar. Coast. Shelf Sci. 169, 1–14.
Uncles, R.J., Stephens, J.A., Barton, M.L., 1984. Observations of fine-sediment concentration and transport in the turbidity maximum region of an estuary. In: Prandle, D. (Ed.), Coastal and Estuarine Studies. Dynamics and Exchanges in Estuaries and the Coastal Zone. American Geophysical Union, pp. 255–276.
van Maren, D.S., Winterwerp, J.C., Vroom, J., 2015. Fine sediment transport into the hyper-turbid lower Ems River: the role of channel deepening and sediment-induced drag reduction. Ocean Dyn. 65, 589–605.
Waeles, B., Le Hir, P., Lesueur, P., Delsinne, N., 2007. Modelling sand/mud transport and morphodynamics in the Seine river mouth (France): an attempt using a process-based approach. Hydrobiologia 588, 69–82.
Wang, Z.B., Hoekstra, P., Burchard, H., Ridderinkhof, H., De Swart, H.E., Stive, M.J.F., 2012. Morphodynamics of the Wadden Sea and its barrier island system. Ocean Coast. Manag. 68, 39–57.
Warner, J.C., Geyer, W.R., Lerczak J. A, 2005. Numerical modeling of an estuary: a comprehensive skill assessment. J. Geophys. Res. 110, C05001. http://dx.doi.org/10.1029/2004JC002691.
Willmott, C.J., 1981. On the validation of models. Phys. Geogr. 2, 184–194.
Winterwerp, J.C., 2007. On the sedimentation rate of cohesive sediment. Estuarine and Coastal Fine Sediments Dynamics – Intercoh 2003. Proc. Mar. Sci. 8, 209–226.
Winterwerp, J.C., Wang, Z.B., 2013. Man-induced regime shifts in small estuaries—I: theory. Ocean Dyn. 63, 1279–1292. http://dx.doi.org/10.1007/s10236-013-0662-9.
Yang, Z., Wang, T., Voisin, N., Copping, A., 2015. Estuarine response to river flow and sea-level rise under future climate change and human development. Estuar. Coast. Shelf Sci. 156, 19–30.